PNAS RESEARCH ARTICLE | BIOCHEMISTRY

Calcineurin-fusion facilitates cryo-EM structure determination of a Family A GPCR

Jun Xu[a,1], Geng Chen[b,1], Haoqing Wang[a], Sheng Cao[b], Jie Heng[c], Xavier Deupi[d,e,f], Yang Du[b,2], and Brian K. Kobilka[a,2]

Affiliations are included on p. 6.

Contributed by Brian K. Kobilka; received July 28, 2024; accepted October 12, 2024; reviewed by Osamu Nuriki, Jurgen Wess, and H. Eric Xu

Advances in singe-particle cryo-electron microscopy (cryo-EM) have made it possible to solve the structures of numerous Family A and Family B G protein-coupled receptors (GPCRs) in complex with G proteins and arrestins, as well as several Family C GPCRs. Determination of these structures has been facilitated by the presence of large extramembrane components (such as G protein, arrestin, or Venus flytrap domains) in these complexes that aid in particle alignment during the processing of the cryo-EM data. In contrast, determination of the inactive state structure of Family A GPCRs is more challenging due to the relatively small size of the seven transmembrane domain (7TM) and to the surrounding detergent micelle that, in the absence of other features, make particle alignment impossible. Here, we describe an alternative protein engineering strategy where the heterodimeric protein calcineurin is fused to a GPCR by three points of attachment, the cytoplasmic ends of TM5, TM6, and TM7. This three-point attachment provides a more rigid link with the GPCR transmembrane domain that facilitates particle alignment during data processing, allowing us to determine the structures of the β_2 adrenergic receptor (β_2AR) in the apo, antagonist-bound, and agonist-bound states. We expect that this fusion strategy may have broad application in cryo-EM structural determination of other Family A GPCRs.

GPCR | cryo-electron microscopy | structure | inactive state

Significance

Advances in cryo-electron microscopy (cryo-EM) have had a major impact on the ability to determine high-resolution structures of G protein-coupled state of G protein-coupled receptors (GPCRs). It has been more challenging to determine the structures of GPCRs in the apo or antagonist-bound inactive states due to challenges in particle orientation. Here, we describe a protein engineering strategy that involves the fusion of calcineurin by three points of attachment to the cytoplasmic ends of TM5, TM6, and TM7 that facilitates particle orientation and structure determination.

GPCRs have been challenging subjects for structural biology for a long time. First, with the exception of bovine rhodopsin, GPCRs are not sufficiently abundant in any mammalian tissue and have to be expressed in heterologous systems (1, 2). Also, most Family A GPCRs are dynamic flexible proteins with little exposed polar surface to facilitate the formation of a crystal lattice(3, 4). Furthermore, most GPCRs are relatively unstable, necessitating long-chain detergents with relatively large micelles (3–5) for efficient purification. Three strategies have been used to overcome these limitations: the development of antibodies that stabilize the GPCR and provide additional polar surfaces (6); thermostabilizing mutations that enable the use of short-chain detergents with smaller micelles (7, 8); and protein engineering to replace the flexible N terminus or intracellular loop (ICL) 3 with highly crystallizable proteins such as T4 Lysozyme and BRIL (9, 10). Nevertheless, crystallization of Family A GPCRs still requires an element of luck and extensive rounds of optimization of the linkers between the receptor and the fusion protein, as well as optimization of crystallization conditions. Moreover, crystallization of GPCRs often depends on the availability of a high-affinity ligand. In contrast, structure determination by cryo-EM is less dependent on luck. If the protein is of sufficient quality, stability, and size, a structure will likely be obtained. In this work, we sought to develop a protein engineering strategy that would enable the use of cryo-EM to determine structures of inactive-state Family A GPCRs that does not require the development of receptor-specific antibodies or nanobodies.

We chose to extend the ICL3 fusion protein strategy previously developed for crystallography (9) by adding an additional link through the C-terminus. We expected that the incorporation of a third link between the soluble protein and the receptor would reduce the flexibility between the two proteins and thereby improve its use as a fiducial marker for the 7TM core. This could be accomplished with a single protein having two or more independently folded domains or with two proteins that form a heterodimer (Fig. 1*A*). The proteins would have to have their N- and C-termini in positions that would be compatible with the relative positions of the cytoplasmic ends of TMs 5, 6, and 7 of the GPCR. Calcineurin (CN), composed of CN-A and CN-B subunits (Fig. 1*B*), was selected as our first candidate as it has the added advantage of being a Ca^{2+}-dependent heterodimer (11). As shown in Fig. 1*B*, CN-B interacts with the C-terminal helix of CN-A (the CN-B binding region) in the presence of four Ca^{2+} ions. The link between CN-A and CN-B can

Author contributions: J.X., X.D., Y.D., and B.K.K. designed research; J.X., G.C., H.W., S.C., and J.H. performed research; J.X., H.W., Y.D., and B.K.K. analyzed data; and J.X., Y.D., and B.K.K. wrote the paper.

Reviewers: O.N., Tokyo Daigaku Daigakuin Rigakukei Kenkyuka Seibutsukagaku Senko; J.W., NIH; and H.E.X., Shanghai Institute of Materia Medica Chinese Academy of Sciences.

Competing interest statement: Brian Kobilka is a co-founder of an consultant for ConfometRx. Confometrx has no financial interest in this paper. Brian Kobilka is a co-founder of ConfmetRx.

[1]J.X. and G.C. contributed equally to this work.

[2]To whom correspondence may be addressed. Email: yangdu@cuhk.edu.cn or kobilka@stanford.edu.

This article contains supporting information online at https://www.pnas.org/lookup/suppl/doi:10.1073/pnas.2414544121/-/DCSupplemental.

Published November 20, 2024.

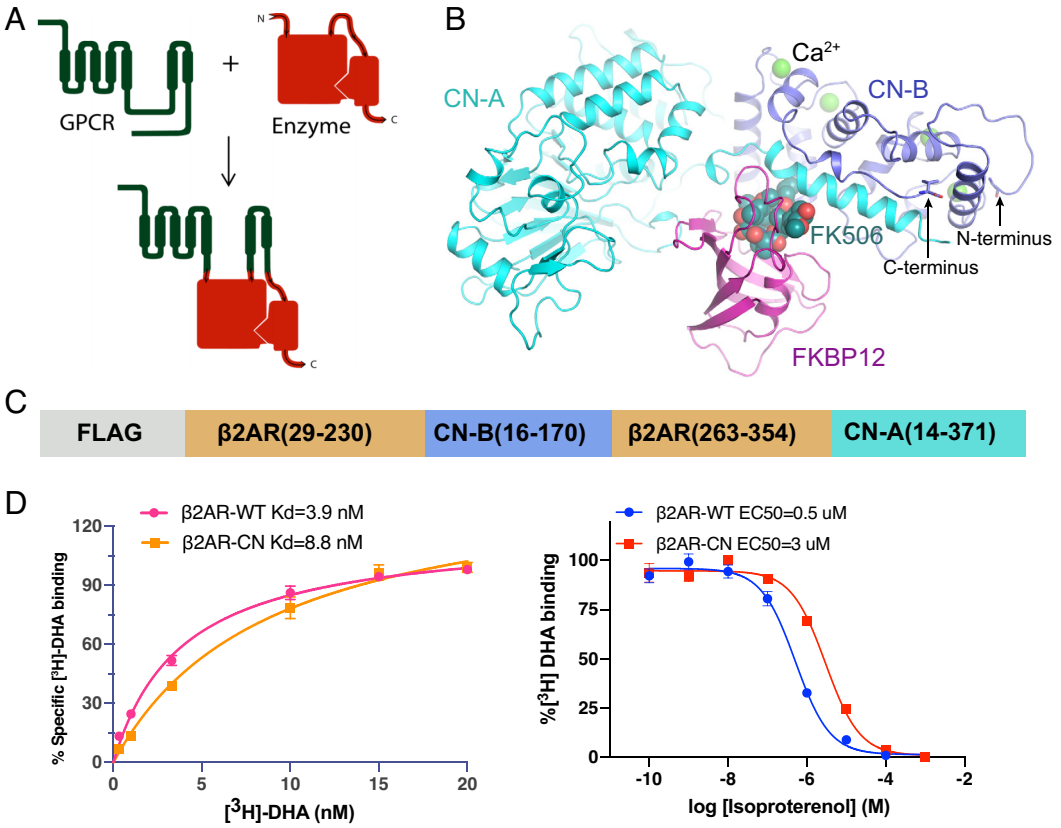

Fig. 1. Engineering of the β2AR-CN fusion protein. (*A*) Concept design of the three-point fusion strategy. (*B*) Structure of the calcineurin heterodimer in complex with FKBP12 and FK506 (PDB: 1TCO). Ca^{2+} atoms are shown as green spheres. (*C*) Optimized construct of the β2AR-CN fusion protein. (*D*) Comparison of the ligand binding properties between the β2AR-CN-fusion construct and WT β2AR. *Left panel*: saturation binding; *Right panel*: competition binding.

be further stabilized by the FK binding protein (FKBP12) in the presence of the inhibitor FK506 (or Tacrolimus) (Fig. 1*B*).

While the N- and C-termini of CN-B are 19 Å apart in the structure of CN-FKBP12 (12), the N terminus is a 15 amino acid long flexible loop that could be conceivably shortened to accommodate the 11 Å distance between the cytoplasmic ends of TM5 and TM6 in the β_2AR (Fig. 1*B*). Our initial construct is shown in *SI Appendix*, Fig. S1*A*, where CN-B (amino acids 16 to 170) is inserted between amino acids 230-263 of the human β_2AR and the CN-A (amino acids 2 to 371) is fused to Y354 in the C-terminus of the β_2AR (*SI Appendix*, Fig. S1*A*). We were able to obtain a well-behaved monomeric fusion protein (*SI Appendix*, Fig. S1 *B* and *C*). 2D averages showed clear architectures for β_2AR, CN-A, and CN-B (*SI Appendix*, Fig. S1*D*). 3D reconstruction finally yielded a map with an overall resolution of 4.2 Å, which showed a relatively rigid orientation between the 7TM of β_2AR and CN (*SI Appendix*, Fig. S1 *E–G*). Of note, computational docking of 3D models into the 4.2 Å map showed that the N-terminal ~15 aa of CN-A lack observable density. This region was also not resolved in the crystal structure, pointing to an intrinsically disordered character (*SI Appendix*, Fig. S1*H*). We further truncated the N terminus of CN-A to create a shorter construct (Fig. 1*C*). Although density in β_2AR is lost after position L341 (*SI Appendix*, Fig. S1*H*), we kept the following residues (342 to 354) to better accommodate the distance between L341 and the N terminus of CN-A. Radioligand binding studies showed that the functional properties of the optimized construct were similar to those of wild-type β_2AR, with almost the same binding affinity for the antagonist carazolol and moderately decreased binding affinity (six fold) for the agonist isoproterenol (Fig. 1*D*).

To further stabilize the conformation of the CN heterodimer, we used the FKBP12 protein to form a complex with β_2AR-CN (*SI Appendix*, Fig. S2*A*). Fig. 2*A* shows a representative 2D class average of the complex, from which we can clearly see all the components of the fusion protein and the FKBP12. We finally reconstructed a 3.5 Å map from the dataset of the β_2AR–CN–FKBP12 complex (*SI Appendix*, Fig. S2 *B–F* and Table S1) that allowed us to build a model for most of the β_2AR, CN-A, CN-B, and FKBP12 (Fig. 2 *B* and *C* and *SI Appendix*, Fig. S2*G*). Densities for the inverse-agonist carazolol and most residues in the orthosteric pocket were well resolved and the ligand can be docked with confidence (Fig. 2 *C* and *D*). We also observed clear density for the compound FK506 which links FKBP12 with CN-A and CN-B (*SI Appendix*, Fig. S2*H*). Moreover, the density for the linkers between CN-B and TM5 and TM6 were well-resolved (Fig. 2*E*). Although we did not observe a continuous density between the C-terminus of the β_2AR and the N terminus of CN-A in the final high-resolution map, the third linker was clearly seen in a well-defined low-resolution map from 3D classification (*SI Appendix*, Fig. S2*I*).

We next compared the cryo-EM structure of carazolol-bound β_2AR with the 2.4 Å crystal structure of the β_2AR-T4L fusion protein (PDB: 2RH1). As expected, the overall structures were similar, with a RMSD of 0.7 Å (Fig. 2*F*). The carazolol binding pockets for the two structures were also highly similar, with a RMSD of 0.5 Å (Fig. 2*G*). The largest difference between the two structures corresponds to intracellular loop 2 (ICL2), which was folded as a helix in the β_2AR-CN cryo-EM structure while it was an unstructured loop in the β_2AR-T4L crystal structure (Fig. 2 *F* and *H*). Existing structures of β_2AR show that ICL2 is a helix in the active state (Fig. 2*H*) and that the transition from a loop to a helix conformation may be an important step for receptor activation (13, 14). Our result suggests that the helical conformation of ICL2 can also exist in the inactive state of β_2AR, possibly in

equilibrium with an unstructured loop conformation. The complete absence of the helical conformation of ICL2 in crystal structures of the inactive β_2AR might be due to crystal lattice contacts with T4L (*SI Appendix*, Fig. S3). Similarly, the slight difference in the conformation of ECL3 may also result from crystal packing (*SI Appendix*, Fig. S3). In addition, we also observed different conformations at the cytoplasmic end of TM6, which was likely caused by the different fusion proteins linked to this helix (Fig. 2*F*).

Although crystallization has enabled the determination of many inactive GPCR structures, most of the successful cases required a high-affinity antagonist or extensive thermostabilization by mutagenesis to make the receptor as stable as possible (3). For most receptors, including the β_2AR, it has not been possible to obtain structures of the apo or agonist-bound receptor alone by crystallography (in the absence of thermostabilizing mutations) due to the inherent dynamics of these states (15). Using the CN-fusion strategy, we were able to obtain the cryo-EM map of the β_2AR in its apo-form and norepinephrine-bound form at 3.9 Å and 3.6 Å, respectively (Fig. 3 *A* and *B* and *SI Appendix*, Figs. S4 and S5 and Table S1). Due to the lower resolution of the apo-state, especially in the extracellular ends of the TM segments and extracellular loops (*SI Appendix*, Fig. S4*D*), many of the side chains could not be modeled; nevertheless, the overall structures of the apo-state and norepinephrine-bound β_2AR were nearly identical to the antagonist-bound structure (Fig. 3*C*). However, local resolution analysis showed that the apo-state receptor was much more flexible than the antagonist-bound or agonist-bound receptor, especially in the orthosteric pocket and extracellular loops (Fig. 3*D*), consistent with the notion that ligand binding stabilizes the conformation around the orthosteric binding pocket. Of note, the TM6 conformation in the norepinephrine-bound structure was the same as the inactive state (Fig. 3*C*). Previously, we obtained a crystal structure of the β_2AR-T4L fusion protein bound to a covalent agonist where TM6 was also in an inactive conformation (16). These results are consistent with fluorescence and spectroscopic studies demonstrating that agonist alone cannot stabilize TM6 of the β_2AR in a fully

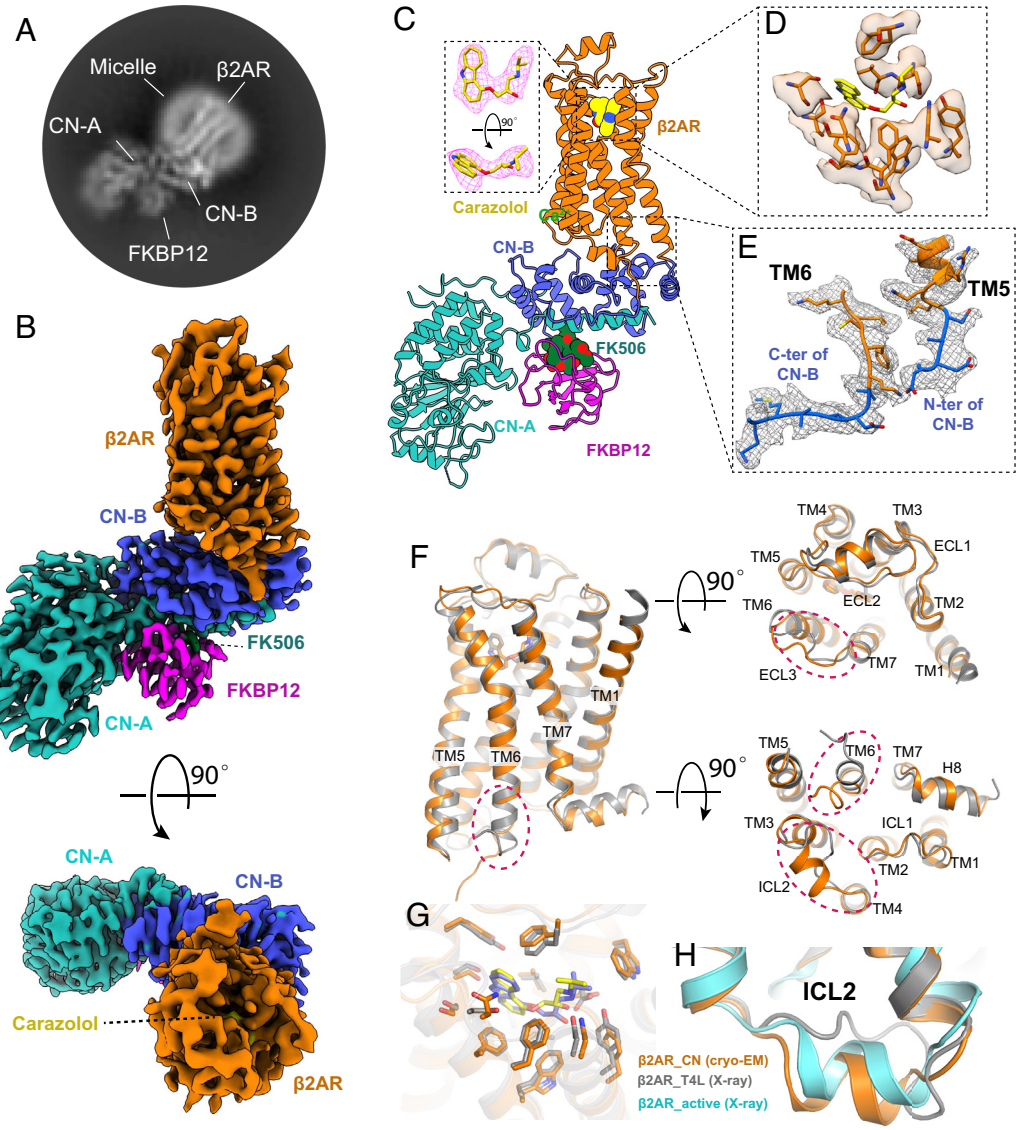

Fig. 2. Cryo-EM structure determination of inverse agonist-bound β2AR using a three-point fusion strategy. (*A*) A representative 2D cryo-EM average of the β2AR–CN-FKBP12 complex shows high-resolution features. (*B*) Cryo-EM density map of the β2AR–CN-FKBP12 complex from side view and top views. (*C*) 3D model of the β2AR–CN-FKBP12 complex. The inset shows the density corresponding to the inverse agonist carazolol depicted as magenta mesh. The map and model in all panels are colored according to polypeptide chains. (*D* and *E*) Density maps and models of the residues in the orthosteric binding pocket (*D*) and the TM5/TM6 linkers between β2AR and CN-B (*E*). (*F*) Overall structural comparison between the cryo-EM structure (orange) and X-ray crystal structure (gray) of the β_2AR. Differences are highlighted with red circles. (*G*) Comparison of the carazolol binding pocket between the cryo-EM and crystal structures. (*H*) Comparison of the ICL2 conformation between inactive and active structures.

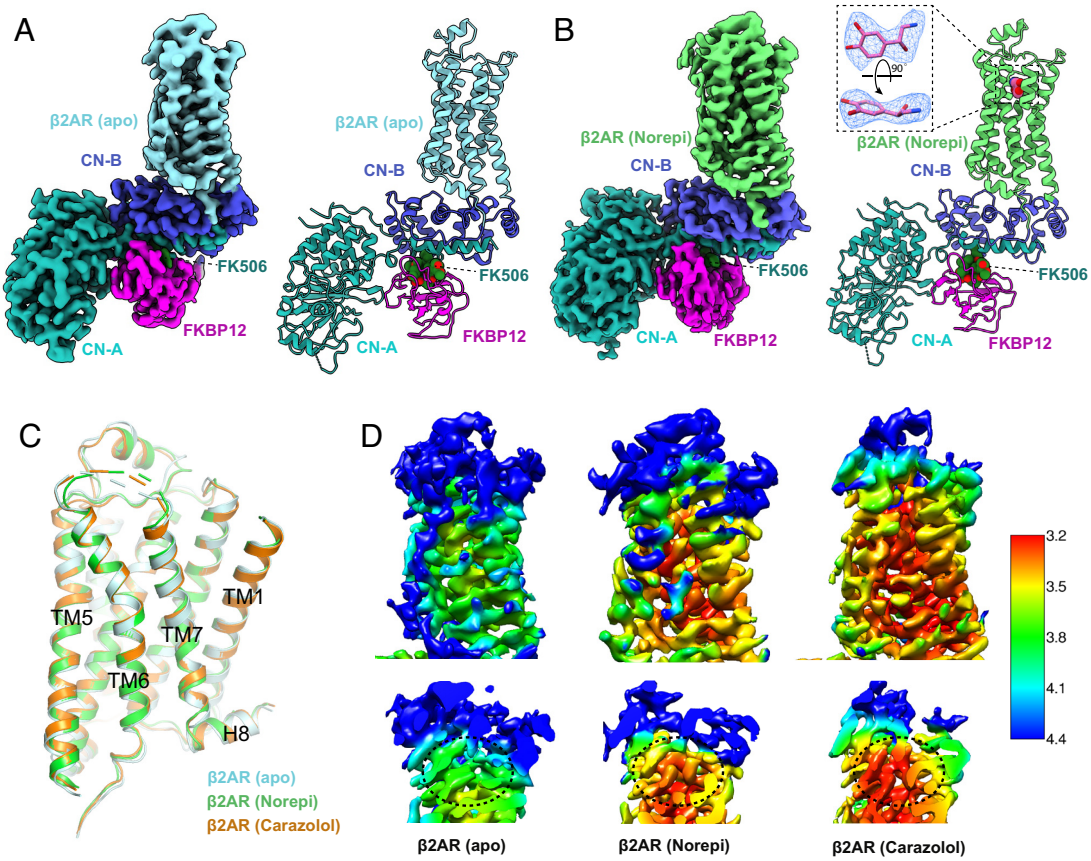

Fig. 3. Cryo-EM structure determination of apo-state and agonist-bound β2AR using the CN fusion strategy. (*A* and *B*) Three-dimensional maps and models of the β2AR–CN-FKBP12 complex in apo (*A*) and norepinephrine-bound (*B*) states. The density map for norepinephrine is shown in the inset as a blue mesh. (*C*) Superimposition of the β2AR structures in apo (cyan), norepinephrine-bound (green), and carazolol-bound (orange) states. (*D*) Comparison of the local resolution maps of the β2AR in apo, norepinephrine-bound, and carazolol-bound states. The orthosteric binding pocket is highlighted with black circles in the *Bottom panels*.

active conformation (15, 17). It's also possible that the CN-fusion stabilizes the inactive conformation of TM6.

Pharmacological studies have revealed that agonists of GPCRs have at least two binding modes: a low-affinity binding mode in the absence of intracellular proteins (e.g., G protein, arrestin, or nanobody) and a high-affinity binding mode when coupled to intracellular binders (18, 19). This can be explained by the model of allosteric coupling between the intracellular signaling proteins and the ligand-binding pocket (18). Indeed, numerous biophysical studies have revealed the conformational changes stabilized by the intracellular protein propagate to the extracellular ligand binding site of GPCRs (20, 21). The norepinephrine-bound inactive β_2AR structure, together with the previously determined active β_2AR crystal structure bound to epinephrine—a nearly identical ligand—and stabilized by a G protein mimetic nanobody (14) allowed us to compare the two states (low affinity and high affinity). For the norepinephrine-bound structure, densities for the ligand and orthosteric pocket residues were relatively well-defined (Figs. 3*B* and Fig. 4*A*). Comparison of the inactive and active structures showed that there is a 1.5 to 2 Å inward movement for TM5 and TM6 in the pocket upon binding with a G protein mimetic nanobody (Fig. 4*B*). The contraction of TM5 and TM6 results in different polar interactions between the ligand and receptor (Fig. 4 *C* and *D*). The amino-ethanol group of norepinephrine/epinephrine forms similar hydrogen-bonding interactions with D113$^{3.32}$ and N312$^{7.39}$ in both states (Fig. 4 *C* and *D*). In the active state, the meta-hydroxyl can form hydrogen bonds with both S203$^{5.42}$ and N293$^{6.55}$ while the para-hydroxyl forms hydrogen bond with S207$^{5.46}$. S204$^{5.43}$ was also involved in the polar network through a hydrogen-bonding interaction with N293$^{6.55}$, which further stabilized the interactions between TM5/6 and the ligand (Fig. 4*D*). In contrast, in the inactive state, norepinephrine can only form a weak hydrogen bond (~3.5 Å) with S203$^{5.42}$ through the para-hydroxyl, which results in much weakened overall interactions between receptor and the ligand (Fig. 4*C*). Together, these results provide a direct structural explanation for the distinct binding affinity of an agonist in the absence and presence of G protein or G protein mimetic nanobody.

In summary, we have developed a protein engineering strategy for structural determination of GPCRs using cryo-EM, in which the heterodimer protein calcineurin was fused to a GPCR by three points of attachment. We demonstrated the feasibility of this method by solving the antagonist-bound inactive structure of the β_2AR. Moreover, we showed that this fusion strategy can also be utilized to determine the structure of receptors in the apo-state and bound to a low-affinity agonist. Recently, a similar three-point fusion strategy has also been used to determine the high-resolution structure of a glucose transporter by fusion of a GFP to the intracellular loop and a GFP-binding nanobody to the C-terminus (22). Although this particular study used two different proteins interacting with each other, these results, together with our calcineurin-fusion strategy, suggest that the three-points fusion strategy might provide a more rigid fiducial maker for particle alignment of small integral membrane proteins during cryo-EM data processing. However, one might still need to optimize the three linkers to get the fusion protein as rigid as possible without affecting the receptor activity. While this might be a time-consuming step, the β_2AR-CN design can be used as an initial template for most of other Family A GPCRs through

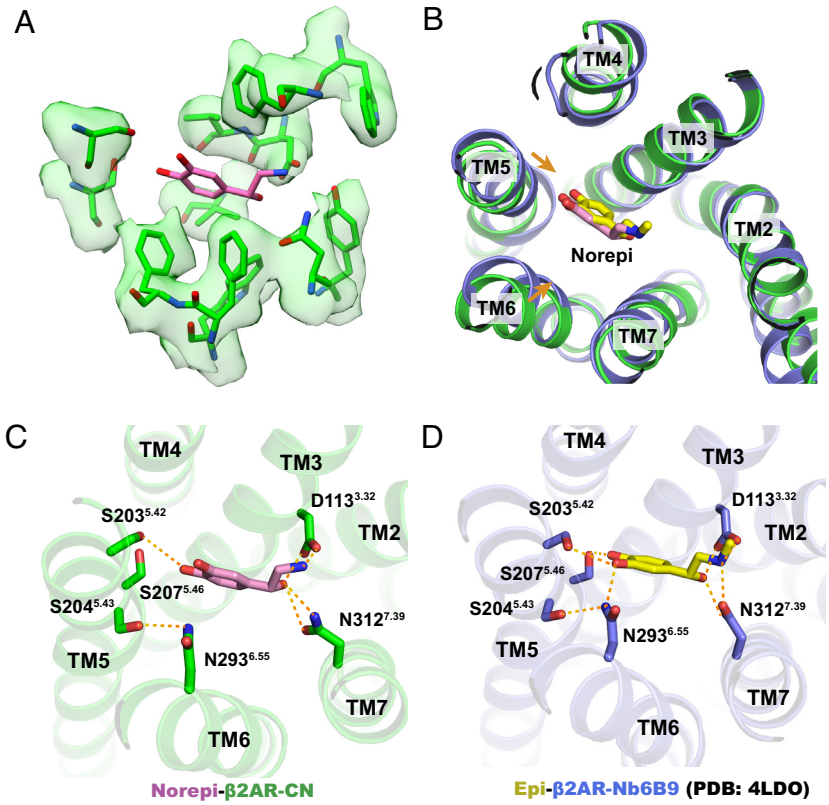

Fig. 4. Comparison of agonist binding modes in inactive and active states. (*A*) Density map and model of the norepinephrine-bound orthosteric pocket residues. (*B*) Comparison of the orthosteric binding pockets of norepinephrine-bound inactive structure and epinephrine-bound active structure. (*C* and *D*) Detailed polar interactions between norepinephrine with inactive β2AR and epinephrine with active β2AR.

simple sequence alignment. Also, along with the emergence of Alphafold2 (23), the predicted three-dimensional model of target receptors can also be used to align with the β_2AR-CN structural model to guide the initial design of CN insertion positions. While preparing our manuscript, other groups have also demonstrated the feasibility of additional fusion strategies, such as BRIL-fusion and PGS fusion, for determining the inactive state structures of GPCRs using cryo-EM (24, 25). It should be noted that higher-resolution GPCR maps were obtained in a recent published study where a small universal nanobody was used as a fiducial maker for cryo-EM analysis (26). This is probably due to the more rigid nanobody-bound receptor complex. Indeed, the local resolution map of β_2AR-CN shows much better resolution of the CN than of the β_2AR (*SI Appendix*, Figs. S2*F*, S4*D*, and S5*D*), indicating that there is still flexibility between CN and receptor. Additional optimization of the linkers may be helpful to further rigidify the fusion protein and to improve the resolution. We believe that this approach may have broad applications in determining the structures of other Family A GPCRs in apo-state or ligand-bound (orthosteric and/or allosteric) state and to facilitate structure-based drug development targeting GPCRs.

Methods

Expression and Purification of FKBP12. The human FKBP12 gene was cloned into pGEX-2TK vector with a C-terminal 6× His tag. Plasmids were transformed into *E. coli* BL21(DE3) cells. Cells were grown to A600 = 0.8 at 37 °C in TB media containing 0.1% glucose, 2 mM $MgCl_2$, and 50 mg/ml ampicillin. Cells were induced by addition of 0.5 mM IPTG and were incubated for 8 h at 37 °C. Cells were harvested and disrupted by sonication. FKBP12 proteins were first purified by Ni-NTA chromatography and then size exclusion chromatography (SEC) with a buffer containing 20 mM HEPEs pH 7.5, 100 mM NaCl, 100 μM TCEP, and 5 μM FK506. Monodisperse peak fractions were collected and concentration using a 3 kDa molecular weight cutoff Millipore concentrator to a concentration at around 15 mg/ml. The concentrated FKBP12 were aliquoted, flash-frozen in liquid nitrogen, and stored at −80 °C before use.

Expression and Purification of β2AR-CN. The human β2AR fused with mouse calcineurin sequence was cloned into pFastBac vector with a N-terminal FLAG tag. Recombinant baculovirus for insect cell expression was made using the Bac-to-Bac system. Sf9 cells were grown in SIM SF Medium (Sino Biological Inc.) at 27 °C and were infected with recombinant baculovirus containing β2AR-CN gene at a density of 4×10^6 cells per mL in the presence of 2 μM alprenolol. After 48 h infection, the cells were spun down and cell pellets were stored at −80 °C until use. Thawed cell pellets were resuspended in a lysis buffer composed of 10 mM Tris, 1 mM EDTA, 10 μM carazolol or 100 μM norepinephrine, 2.5 μg/mL leupeptin, and 160 μg/mL benzamidine to lyse the cells by hypotonic. Cell membranes were then spun down and solubilized with a buffer of 20 mM HEPEs pH 7.5, 100 mM NaCl, 1 % DDM, 0.03 % CHS, 2.5 μg/mL leupeptin, 160 μg/mL benzamidine, 5 mM $CaCl_2$, and 10 μM carazolol or 100 μM norepinephrine at 4 °C for 1 h. The solubilized receptor was then loaded onto a column with anti-flag M1 affinity resin and was extensively washed with a buffer containing 20 mM HEPEs, pH 7.5, 300 mM NaCl, 0.1 % DDM, 0.003 % CHS, 2 mM $CaCl_2$, and 10 μM carazolol or 100 μM norepinephrine. The receptor was then gradually exchanged into a buffer containing 20 mM HEPEs pH 7.5, 100 mM NaCl, 0.0075% lauryl maltose neopentyl glycol (LMNG, Anatrace), 0.0025%GDN, 0.001% CHS, 2 mM $CaCl_2$, and 10 μM carazolol or 100 μM norepinephrine and then eluted with same buffer supplemented with 0.2 mg/ml flag peptide and 5 mM EDTA. The flag affinity chromatography purified receptor was supplemented with 10 mM $CaCl_2$ immediately, then concentrated to 500 μL and finally purified by SEC chromatography with a buffer containing 20 mM HEPEs pH 7.5, 100 mM NaCl, 0.00075%LMNG, 0.00025%GDN, 0.0001% CHS, 0.5 mM $CaCl_2$, and 10 μM carazolol or 100 μM norepinephrine. The monodisperse peak fractions were collected and concentrated to ~10 mg/ml for cryo-EM analysis. For complexing with FKBP12, the monodisperse peak fractions were collected and incubated with excess FKBP12 in the presence of 5 μM FK506 for 1 h on ice. The β2AR–CN–FKBP12 mix was then subjected to SEC chromatography against a buffer containing 20 mM HEPEs pH 7.5, 100 mM NaCl,

0.00075%LMNG, 0.00025%GDN, 0.0001% CHS, 0.5 mM $CaCl_2$, 10 μM carazolol or 100 μM norepinephrine, and 5 μM FK506. The complex peak was collected and concentrated to ~10 mg/ml for cryo-EM. For the apo-state sample, no ligand was added in expression and all purification steps.

Cryo-EM Sample Preparation and Data Collection. For carazolol and norepinephrine–bound samples, amorphous alloy film (CryoMatrix nickel titanium alloy film, R1.2/1.3, Zhenjiang Lehua Electronic Technology Co., Ltd.) was glow-discharged for 60 s at a Tergeo-EM plasma cleaner. Then, 3 μL purified β_2AR-CN or β_2AR–CN–FKBP12 sample was applied onto the grid and then blotted for 3 s with blotting force 0 and quickly plunged into liquid ethane cooled by liquid nitrogen using Vitrobot Mark IV (Thermo Fisher Scientific) at 4 °C and with 100% humidity. Cryo-EM data were collected on a 300 kV Titan Krios Gi3 microscope. The raw movies were recorded by Gatan K3 BioQuantum Camera at a magnification of 105 000, and a pixel size of 0.85 Å. Inelastically scattered electrons were excluded by a GIF Quantum energy filter (Gatan) using a slit width of 20 eV. The movie stacks were acquired with a defocus range of −1.0 to −1.6 micron with a total exposure time 2.5 s fragmented into 50 frames (0.05 s/frame) and with a dose rate of 22.0 e/pixel/s. The imaging mode was super resolution with 2-time hardware binning. Semiautomatic data acquisition was performed using SerialEM.

For the apo-state sample, a Quantifoil grid (R1.2/1.3, Au) was glow-discharged for 45 s at easiGlow discharged cleaning system. An aliquot of 3 μL sample was deposited onto the grid and plunge-frozen into liquid ethane using an Vitrobot Mark IV. Data collection was conducted on Titan Krios operated at 300 keV using a nominal magnification of 130,000×. Movies were captured using a Gatan K3 Summit direct electron detector in counted mode, which resulted in a pixel size of 0.85 Å. Movie stacks were obtained with a defocus range of −1.0 to −2.0 μm, using SerialEM 3.7.10 with a set of customized scripts enabling automated low-dose image acquisition. Each movie stack was recorded for a total of 8 seconds with 0.2 s per frame. The exposure rate was 7 electrons per pixel per second.

Cryo-EM Image Analysis and Model Building. The image stacks of the β_2AR-CN fusion protein were collected and subjected for motion correction using MotionCor2 (27). Contrast transfer function parameters were estimated by CTFFIND4 (28), implemented in RELION3.1 (29). Then, 2,000 particles were manually picked and extracted from the motion-corrected micrographs followed with 2D classification. Templates were selected from the 2D classification result. Particles were autopicked using the templates in RELION and then subjected to 2D classification using cryoSPARC (30). Selected particles with appropriate 2D average from 2D classification were further subjected to Ab initio reconstruction. Particles with appropriate initial model were selected from Ab initio followed by homogeneous refinement in cryoSPARC. After global and local CTF refinement, the particles (kept to 325′064) were subjected to nonuniform refinement for a 4.20 Å reconstruction determined by gold standard Fourier shell correlation using the 0.143 criterion. Data processing for the β_2AR–CN–FKBP12 complexes was done in cryoSPARC. For the carazolol-bound β_2AR–CN–FKBP12 complex, a total of 6′001 image stacks were collected and subjected to patch motion correction and patch CTF refinement. Further, 2′819′890 particles were autopicked using the β_2AR-CN map as a template and then subjected to 2D classification followed by Ab initio reconstruction and 2 rounds of heterogeneous refinement. The resulting particles were subject to nonuniform refinement and local refinement and yielded a map at 3.6 Å. After local motion correction and another round of nonuniform refinement and local refinement, the resolution was improved to 3.49 Å. The norepinephrine-bound and apo-state datasets were processed in a similar way as the carazolol-bound dataset (*SI Appendix*, Figs. S4*B* and S5*B*). The crystal structure of the inactive β_2AR (PDB code: 2RH1), rat calcineurin (PDB code: 4IL1), and FKBP12-FK506 (PDB code: 1FKJ) were used as initial models for model rebuilding and refinement against EM density map. The models were docked into the EM density map using UCSF Chimera (31), followed by iterative manual building in Coot (32) and refinement in Phenix (33).

Radio-Ligand Binding Assay. SF9 insect cell membranes were prepared following a previously reported protocol (34). Radioligand saturation binding of the antagonist [^{3}H]-dihydroalprenolol (PerkinElmer) was conducted with the cell membranes to a final volume of 250 μL. Briefly, the cell membranes were diluted in assay buffer containing 20 mM Hepes, pH 7.4, 100 mM NaCl, and 0.5 mg/mL BSA. Serial dilutions of [^{3}H]-dihydroalprenolol at indicated final concentrations were incubated with the membranes for 1.5 h while shaking at 200 rpm at room temperature. The membranes were washed and collected by filtration with a 48-well Brandel harvester. The filter papers containing the membrane were incubated with a 3 mL OptiPhase HiSafe 3 liquid scintillation cocktail. Radioactivity was counted with a Microbeta2 scintillation counter. All curves were constructed from mean ± SEM of three independent experiments at three replicas, and the saturation binding data were analyzed in GraphPad Prism software using a one-site saturation binding equation. For radioligand competition binding, membrane solutions were incubated with 2 nM [^{3}H]-dihydroalprenolol and the unlabeled competitor to a final volume of 250 μL. The assay buffer contains 20 mM Hepes, pH 7.4, 100 mM NaCl, and 0.5 mg/mL BSA. Binding reactions were incubated and shaken at room temperature for 1.5 h and were harvested using a 48-well Brandel harvester. All curves were constructed from mean ± SEM of three independent experiments at three replicas. Competition binding data were analyzed in GraphPad Prism software using a one-site competitive binding equation.

Data, Materials, and Software Availability. The 3D cryo-EM density maps have been deposited in the Electron Microscopy Data Bank under accession code EMD-45604 (35), EMD-45602 (36), and EMD-45603 (37) for carazolol-bound, norepi-bound, and apo states, respectively. The atomic coordinates for the atomic models generated in this study have been deposited in the Protein Data Bank under accession code 9CHX (38), 9CHU (39), and 9CHV (40) for carazolol-bound, norepi-bound and apo states, respectively. All other study data are included in the manuscript and/or *SI Appendix*.

ACKNOWLEDGMENTS. We would like to thank the Cryo-EM Center of the Chinese University of Hong Kong, Shenzhen for data collection. Some CryoEM data collection was performed at the Stanford-SLAC Cryo-EM Facilities, supported by Stanford University, SLAC, and the NIH S10 Instrumentation Programs. We thank Elizabeth Montabana, Chensong Zhang, and Dr. Zheng Liu for their support on CryoEM data collection. Part of CryoEM data processing for this project was performed on the Sherlock cluster. We would like to thank Stanford University and the Stanford Research Computing Center for providing computational resources and support that contributed to these research results. Y.D. is supported by grants from Science, Technology and Innovation Commission of Shenzhen Municipality (Project code 10120210014) and in part by the startup fund of Institute of Innovative Drug Discovery, Chinese University of Hong Kong, Shenzhen. This work was also supported by the American Heart Association Postdoctoral Fellowship (H.W.). B.K.K. was a Chan Zuckerberg Biohub Investigator and received funding from R01NS028471.

Author affiliations: [a]Department of Molecular and Cellular Physiology, Stanford University School of Medicine, Stanford, CA 94305; [b]Kobilka Institute of Innovative Drug Discovery, School of Medicine, Chinese University of Hong Kong, Shenzhen, Guangdong 518172, China; [c]Beijing Advanced Innovation Center for Structural Biology, School of Medicine, Tsinghua University, Beijing 100084, China; [d]Condensed Matter Theory Group, Division of Scientific Computing, Theory, and Data, Paul Scherrer Institute, 5232 Villigen, Switzerland; [e]Laboratory of Biomolecular Research, Division of Biology and Chemistry, Paul Scherrer Institute, 5232 Villigen, Switzerland; and [f]Swiss Institute of Bioinformatics, Lausanne, Switzerland

1. K. Palczewski *et al.*, Crystal structure of rhodopsin: A G protein-coupled receptor. *Science* **289**, 739–745 (2000).
2. S. Granier, B. Kobilka, A new era of GPCR structural and chemical biology. *Nat. Chem. Biol.* **8**, 670–673 (2012).
3. S. C. Erlandson, C. McMahon, A. C. Kruse, Structural basis for G protein–coupled receptor signaling. *Annu. Rev. Biophys.* **47**, 1–18 (2018).
4. B. K. Kobilka, X. Deupi, Conformational complexity of G-protein-coupled receptors. *Trends in Pharmacol. Sci.* **28**, 397–406 (2007).
5. A. Manglik, B. Kobilka, The role of protein dynamics in GPCR function: Insights from the beta2AR and rhodopsin. *Curr. Opin. Cell Biol.* **27**, 136–143 (2014).
6. S. G. Rasmussen *et al.*, Crystal structure of the human beta2 adrenergic G-protein–coupled receptor. *Nature* **450**, 383–387 (2007).
7. T. Warne *et al.*, Structure of a beta1-adrenergic G-protein-coupled receptor. *Nature* **454**, 486–491 (2008).
8. M. J. Serrano-Vega, F. Magnani, Y. Shibata, C. G. Tate, Conformational thermostabilization of the beta1-adrenergic receptor in a detergent-resistant form. *Proc. Natl. Acad. Sci. U.S.A.* **105**, 877–882 (2008).

9. D. M. Rosenbaum *et al.*, GPCR engineering yields high-resolution structural insights into beta2-adrenergic receptor function. *Science* **318**, 1266–1273 (2007).
10. E. Chun *et al.*, Fusion partner toolchest for the stabilization and crystallization of G protein-coupled receptors. *Structure* **20**, 967–976 (2012).
11. H. Li, A. Rao, P. G. Hogan, Interaction of calcineurin with substrates and targeting proteins. *Trends Cell Biol.* **21**, 91–103 (2011).
12. J. P. Griffith *et al.*, X-ray structure of calcineurin inhibited by the immunophilin-immunosuppressant FKBP12-FK506 complex. *Cell* **82**, 507–522 (1995).
13. X. Y. Liu *et al.*, Mechanism of beta(2)AR regulation by an intracellular positive allosteric modulator. *Science* **364**, 1283 (2019).
14. A. M. Ring *et al.*, Adrenaline-activated structure of beta(2)-adrenoceptor stabilized by an engineered nanobody. *Nature* **502**, 575 (2013).
15. A. Manglik *et al.*, Structural insights into the dynamic process of beta(2)-adrenergic receptor signaling. *Cell* **161**, 1101–1111 (2015).
16. D. M. Rosenbaum *et al.*, Structure and function of an irreversible agonist-beta(2) adrenoceptor complex. *Nature* **469**, 236–240 (2011).
17. G. G. Gregorio *et al.*, Single-molecule analysis of ligand efficacy in β2AR-G-protein activation. *Nature* **547**, 68–73 (2017).
18. B. T. DeVree *et al.*, Allosteric coupling from G protein to the agonist-binding pocket in GPCRs. *Nature* **535**, 182–186 (2016).
19. T. Warne, P. C. Edwards, A. S. Dore, A. G. W. Leslie, C. G. Tate, Molecular basis for high-affinity agonist binding in GPCRs. *Science* **364**, 775–778 (2019).
20. S. Isogai *et al.*, Backbone NMR reveals allosteric signal transduction networks in the beta1-adrenergic receptor. *Nature* **530**, 237–241 (2016).
21. J. Xu *et al.*, Conformational complexity and dynamics in a muscarinic receptor revealed by NMR spectroscopy. *Mol. Cell* **75**, 53–65.e7 (2019).
22. Y. Niu *et al.*, Structural basis of inhibition of the human SGLT2-MAP17 glucose transporter. *Nature* **601**, 280–284 (2022).
23. D. Sala, P. W. Hildebrand, J. Meiler, Biasing AlphaFold2 to predict GPCRs and kinases with user-defined functional or structural properties. *Front. Mol. Biosci.* **10**, 1121962 (2023).
24. K. Zhang, H. Wu, N. Hoppe, A. Manglik, Y. Cheng, Fusion protein strategies for cryo-EM study of G protein-coupled receptors. *Nat. Commun.* **13**, 4366 (2022).
25. Q. Guo *et al.*, A method for structure determination of GPCRs in various states. *Nat. Chem. Biol.* **20**, 74 (2024).
26. M. J. Robertson *et al.*, Structure determination of inactive-state GPCRs with a universal nanobody. *Nat. Struct. Mol. Biol.* **29**, 1188–1195 (2022).
27. S. Q. Zheng *et al.*, MotionCor2: Anisotropic correction of beam-induced motion for improved cryo-electron microscopy. *Nat. Methods* **14**, 331–332 (2017).
28. A. Rohou, N. Grigorieff, CTFFIND4: Fast and accurate defocus estimation from electron micrographs. *J. Struct. Biol.* **192**, 216–221 (2015).
29. S. H. Scheres, RELION: Implementation of a Bayesian approach to cryo-EM structure determination. *J. Struct. Biol.* **180**, 519–530 (2012).
30. A. Punjani, J. L. Rubinstein, D. J. Fleet, M. A. Brubaker, cryoSPARC: Algorithms for rapid unsupervised cryo-EM structure determination. *Nat. Methods* **14**, 290–296 (2017).
31. E. F. Pettersen *et al.*, UCSF Chimera–a visualization system for exploratory research and analysis. *J. Comput. Chem.* **25**, 1605–1612 (2004).
32. P. Emsley, B. Lohkamp, W. G. Scott, K. Cowtan, Features and development of Coot. *Acta Crystallographica. Section D, Biol. Crystallography* **66**, 486–501 (2010).
33. P. D. Adams *et al.*, PHENIX: A comprehensive Python-based system for macromolecular structure solution. *Acta Crystallogr. Section D, Biol. Crystallogr.* **66**, 213–221 (2010).
34. X. Xu *et al.*, Binding pathway determines norepinephrine selectivity for the human β1AR over β2AR. *Cell Res.* **31**, 569–579 (2020).
35. J. Xu, G. Chen, Y. Du, B. K. Kobilka, Cryo-EM structure of calcineurin-fused beta2 adrenergic receptor in carazolol bound inactive state. Electronic Microscopy Data Bank. https://www.ebi.ac.uk/emdb/EMD-45604. Deposited 2 July 2024.
36. J. Xu, G. Chen, Y. Du, B. K. Kobilka, Cryo-EM structure of calcineurin fused beta2 adrenergic receptor in norepinephrine bound inactive state. Electronic Microscopy Data Bank. https://www.ebi.ac.uk/emdb/EMD-45602. Deposited 2 July 2024.
37. J. Xu, G. Chen, Y. Du, B. K. Kobilka, Cryo-EM structure of calcineurin-fused beta2 adrenergic receptor in apo state. Electronic Microscopy Data Bank. https://www.ebi.ac.uk/emdb/EMD-45603. Deposited 2 July 2024.
38. J. Xu, G. Chen, Y. Du, B. K. Kobilka, Cryo-EM structure of calcineurin-fused beta2 adrenergic receptor in carazolol bound inactive state. Protein Data Bank. https://www.rcsb.org/structure/9CHX. Deposited 2 July 2024.
39. J. Xu, G. Chen, Y. Du, B. K. Kobilka, Cryo-EM structure of calcineurin fused beta2 adrenergic receptor in norepinephrine bound inactive state. Protein Data Bank. https://www.rcsb.org/structure/9CHU. Deposited 2 July 2024.
40. J. Xu, G. Chen, Y. Du, B. K. Kobilka, Cryo-EM structure of calcineurin-fused beta2 adrenergic receptor in apo state. Protein Data Bank. https://www.rcsb.org/structure/9CHV. Deposited 2 July 2024.